energies

MDPI

Article

Graphite Regeneration and NCM Cathode Type Synthesis from Retired LIBs by Closed-Loop Cycle Recycling Technology of Lithium-Ion Batteries

Alexandra Kosenko *, Konstantin Pushnitsa, Vladislav Chernyavsky, Pavel Novikov and Anatoliy A. Popovich

Laboratory "Synthesis of the New Materials and Structures", Peter the Great Saint-Petersburg Polytechnic University, 195221 Saint Petersburg, Russia
* Correspondence: alxndra.kosenko@gmail.com

Abstract: A closed-loop regeneration process for spent $LiCoO_2$ has been successfully designed with prior synthesis of $LiNi_xCo_yMn_zO_2$, by the authors. This research applies the methodology to lithium-ion battery anodes, using spent graphite from a decommissioned battery in a leaching process with 1.5 mol·L^{-1} malic acid and 3% H_2O_2 alongside $LiCoO_2$. The filtered graphite was separated, annealed in an argon atmosphere, and the filtrate was used to synthesize NCM cathode material. Characterization involved X-ray diffraction, EDX, and SEM techniques. The regenerated graphite (RG) showed a specific discharge capacity of 340.4 mAh/g at a 0.1C rate in the first cycle, dropping to 338.4 mAh/g after 55 cycles, with a Coulombic efficiency of 99.9%. CV and EIS methods provided further material assessment. In a related study, the SNCM111 synthesized from the leaching solution showed a specific discharge capacity of 131.68 mAh/g initially, decreasing to 115.71 mAh/g after 22 cycles.

Keywords: spent graphite anode; regeneration; $LiCoO_2$; NCM cathode; retired lithium-ion batteries; recycling

check for updates

Citation: Kosenko, A.; Pushnitsa, K.; Chernyavsky, V.; Novikov, P.; Popovich, A.A. Graphite Regeneration and NCM Cathode Type Synthesis from Retired LIBs by Closed-Loop Cycle Recycling Technology of Lithium-Ion Batteries. *Energies* **2024**, *17*, 5570. https://doi.org/10.3390/en17225570

Academic Editors: Anup Barai, Sheikh Muhammad and Mohammad Al-Amin

Received: 16 October 2024
Revised: 30 October 2024
Accepted: 5 November 2024
Published: 7 November 2024

Copyright: © 2024 by the authors. Licensee MDPI, Basel, Switzerland. This article is an open access article distributed under the terms and conditions of the Creative Commons Attribution (CC BY) license (https://creativecommons.org/licenses/by/4.0/).

1. Introduction

Over the past two decades, the proliferation of lithium-ion batteries (LIBs) has surged, driven by their diverse applications. However, the typical lifecycle of these batteries is approximately 3 to 5 years [1], which forecasts an exponential increase in retired LIBs. Some researchers estimate that global LIB waste may exceed 460,000 tons by 2025 and approximately 11 million tons by 2030 [2].

Historically, research on lithium-ion recycling has predominantly concentrated on cathode material regeneration and metal recovery, as the most valuable and precious components (e.g., lithium, copper, aluminum, manganese, and nickel) are contained in it [3,4].

Graphite is a carbon-based mineral distinguished by its hexagonal layered structure, which exhibits weak van der Waals interactions that promote the embedding and removal of lithium ions, resulting in the formation of graphite intercalation compounds (GICs). Graphitic materials have low working potential plateaus (approximately 0.15 V vs. Li+/Li), a theoretical capacity of up to 372 mAh·g^{-1}, thermal and mechanical stability, low expansion value, and highly crystalline structure; consequently, they are extensively employed as anode materials in commercial lithium-ion batteries [5–7]. However, the crystal structure of graphite can deteriorate with repeated charging and discharging cycles, compounded by impurities such as PVDF binder and solid electrolyte interphase film, which primarily consist of various lithium compounds [8,9]. This degradation can lead to a significant decline in graphite capacity, necessitating appropriate treatment or regeneration processes for effective reuse [10].

The lack of established graphite recovery technologies has resulted in the disposal of spent graphite as waste, thus leading to resource loss and environmental contamination [11,12]. However, it is crucial to emphasize that the quantity of graphite utilized in lithium-ion batteries (LIBs) typically ranges from 10% to 20%, significantly higher than the lithium content by a factor of eleven. This disparity underscores the economic and environmental imperative for developing graphite recycling strategies. Although various studies have investigated this area [13], the global emphasis on graphite recycling remains considerably less pronounced than that on cathode material processing, highlighting the need for further research and development in this domain.

In our early studies of such an essential topic in the field of LIB recycling, we have earlier published a review on the newly investigated methods of graphite recovery, recycling, and reuse [14]. In Table 1, the mainly interesting references are listed.

Table 1. The list of newly investigated methods of graphite anode post-processing.

Process Description	Ref.
1. 5 mol/L H_2SO_4, 35 *w*/*w* %H_2O_2 2. Annealing: 500 °C, 40 min with NaOH additive	[15]
0.2 mol·L^{-1} solution of citric acid, 90 °C, 50 min	[9]
2600 °C, Ar atmosphere	[16]
H_2SO_4 + 1500 °C for 2 h	[17]
1. H_2SO_4 2. Sintering with $Co(NO_3)_2$ at 900 °C for 4 h under N_2	[18]
Electrolysis: 30 V, 1.5 g/L Na_2SO_4, 25 min	[19]
1. Leaching sulfuric acid H_2SO_4, 200 g·L^{-1}, 90 °C, 4 h 2. Microwave radiation 800 W, 15 s	[20]
1. Leaching process with H_2O_2. Microwave radiation 800 W 20–30 s	[21]
1. Leaching with acid usage, annealing at N_2 atmosphere 2. PEG 400 monooleate acid—200 mL, Graphite—1 g Zinc chloride—2 g 1000 °C, 2 h at N_2 atmosphere	[7]
1. Leaching process using acid followed by air annealing. 2. Materials: - Graphite: 10 g - Phenolic resin–ethanol solution: 0.02 L - Solidification: 1 h at 120 °C, followed by 1 h at 950 °C in a nitrogen atmosphere.	[22]
1. N-Methyl-pyrrolidone + scrapping 2. Ball milling with nanosized silicon, 800 °C, 3 h with Ar	[23]
1. Acid leaching for the oxidation of the positive electrode and intercalation in the negative electrode. 2. Solvothermal synthesis at 160 °C for 12 h.	[24]
1. Intercalation process+ scrap 2. Gas sulfidation at 600 °C for 2 h under an Ar/N_2 atmosphere.	[25]
Application in rechargeable batteries: 1. Application in LIB/SIB—Cu-BTC MOF 2. Application in DIB—joint cation-anion RLFPG 3. Application in SIB/KIB—HT spent graphite	 [26] [27] [28]
Application in catalysts: 1. Catalytic redox degradation of organic compounds utilizing spent graphite. 2. Photodegradation of methylene blue—GO/Cuo 3. Heterogeneous Fenton reaction for 4-chlorophenol removal—ZVI-EG	 [29] [30] [31]

Table 1. *Cont.*

Process Description	Ref.
Application in capacitors:	
1. Supercapacitor featuring cobalt–copper nanowire as the positive electrode and graphite as the negative electrode.	[32]
2. Glyme-based Li-ion capacitor with LiC_6	[33]
3. Glyme-based Na-ion capacitor with NaC_6	[34]
4. Li-ion capacitor with LiC_6	[35]
Graphene applications:	
1. Decrease in H_2SO_4 and $KMnO_4$ consumption in graphene synthesis	[36]
2. Decreasing the cost for production of graphene (540$ per ton graphene)	
Li recovery from spent graphite anode	[37]

Based on our previous research on triple-lithiated transition metal cathode material synthesis, it was determined that the methodology should be extended to include anode regeneration. The spent graphite anode contains various compositions, such as LiC_x, LiF, Li_2CO_3, or lithium alkyl carbonates $ROCO_2Li$. Therefore, using acid leaching with 1.5 M malic acid and 3 vol.% H_2O_2 enables the extraction of Li^+ ions into the leachate. Besides the lithium extraction from damaged graphite structure, in order to aim for the exceptional electrochemical characteristics of material after regeneration processes, it is necessary to use high-temperature treatment, which allows for the restoration of the layered crystal structure and enlarges the layer spacing between graphite layers [38,39].

Graphitization is a specific type of solid-phase reaction in which an amorphous material transforms into a crystalline structure. This transformation can be challenging to achieve and often requires elevated temperatures. However, by incorporating certain metals or their compounds, or non-metals and their compounds, graphitization can occur at lower temperatures, a process referred to as catalytic graphitization [40]. In this research, it was decided to conduct the experiment with cobalt malate from cathode material extraction, and to use this salt as a catalyst for graphite regeneration. This approach allows for the separation of black mass—the mix of cathode and anode powders, which is the key problem of any existing industrial recycling technology. To sum up, this study explores the simultaneous leaching of spent anodes and cathodes from retired lithium-ion batteries to establish a closed-loop regeneration process, and the regenerated graphite material and synthesized NCM material from obtained precursors are investigated.

2. Materials and Methods

The initial materials utilized were the anode with a copper current collector and the cathode, along with the aluminum current collector, which has been extracted from a retired lithium-ion battery. The positive electrode served as the primary source of cobalt and lithium, while the negative electrode served as the source of spent graphite. The discharged battery underwent a complete discharge in a 5% NaCl solution for a duration of 24 h, after which it was dismantled, and the electrodes were separated from the other components of the battery.

The electrodes underwent a leaching process in a solution of 1.5 mol/L malic acid with 3 vol.% H_2O_2 at 90 °C while being stirred for 1 h. The role of the malic acid was to transfer the lithium and cobalt ions from the spent electrodes to the water-soluble cobalt and lithium malate. The malic acid was chosen due to its environmentally friendly nature, effectiveness in enhancing target component extraction, and its ability to minimize harmful byproducts. Additionally, malic acid is a biodegradable compound, making it a sustainable alternative to harsher chemical methods, such as inorganic acids. Hydrogen peroxide is the reducing agent in this process. After that, any residue (aluminum and copper foils, PVDF, black carbon) and graphite powder were separated from the solution through filtration, resulting in a solution containing Li^+ and Co^{2+} ions. The further synthesis of regenerated cathode material of NCM type was conducted utilizing the previously mentioned solution, while the filtered graphite powder underwent heat treatment in a tube furnace (Richmond,

CA, USA), at 1100 °C for 4 h in an argon atmosphere to restore its crystalline structure. The choice of annealing conditions was based on a previously carried experiment [41]. The heating speed was 10 °C/min, the gas flow was 20 mL/min, and passive cooling with the furnace.

The NCM synthesis involved several stages. Nickel, manganese, and lithium acetates were mixed into the leachate solution in precise stoichiometric ratios to produce the NCM material. The calculations were performed as follows: after the leaching was completed, the filtered residue was dried for 24 h and weighed. The weight of the residue was then subtracted from the initial mass of the cathode, yielding the theoretical mass of the solubilized cathode material. The value was adjusted by multiplying it by 0.92 to calculate the active mass in the solution. A typical coating ratio of 92:5:3, reflecting the proportions of cathode material, binder (PVDF), and conductive additive, was applied to the current collector. The active mass was multiplied by 0.59 to estimate the theoretical cobalt mass in the solution. This value was then divided by the molar mass of cobalt (59 g/mol) to determine the concentration of Co^{2+} ions. To find the quantity of NCM111, the cobalt amount was tripled. The required masses of nickel (II) acetate tetrahydrate (NiAc), manganese (II) acetate tetrahydrate (MnAc), and lithium acetate dihydrate (LiAc) were calculated based on these amounts, with NiAc and MnAc matching the cobalt mass, while LiAc corresponded to the NCM111 quantity, using their respective molar masses. Lastly, water evaporated from the solution, along with the removal of gas. The precipitate obtained was utilized as a precursor for the subsequent synthesis of SNCM (synthesized NCM) cathode material through the annealing process. The annealing process in more detail is described in Supplementary Materials. A schematic overview of this process is presented in Figure 1.

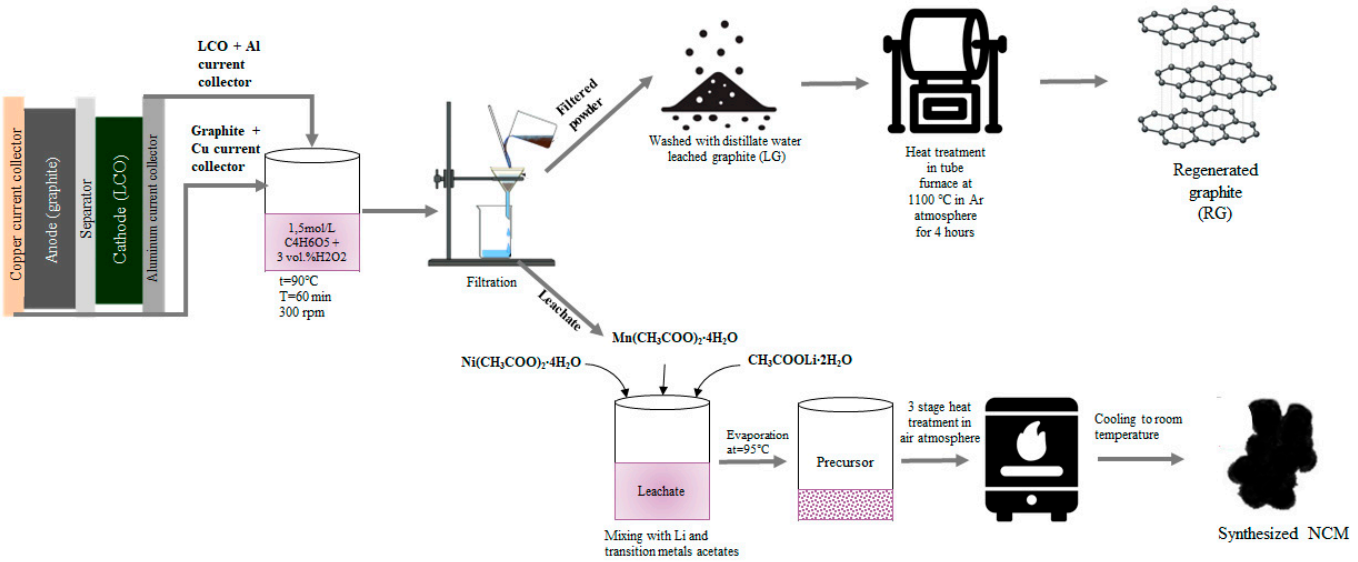


Figure 1. The scheme of closed-loop regeneration process.

A Mira 3 Tescan scanning electron microscope (TESCAN, Brno, Czech Republic) was used to analyze the microstructure and morphology of the obtained powders in secondary electron (SE) mode. The compositional analysis of the samples was assessed via energy-dispersive X-ray spectroscopy EDX Oxford Instruments X-Max 80 (Oxford Instruments, Thane, India). A Bruker D8 Advance diffractometer (Bruker, Billerica, MA, USA), with a CuKα wavelength of 1.5406 Å, scanning in an angle range of 15 to 85 degrees with a step size of 0.030, and an exposure time of 0.8 s per step was utilized to perform X-ray phase analysis of the samples. The composition of the phases was identified with DIFFRAC.EVA V5.0 software, while structural parameters were refined through the Rietveld method using TOPAS5 software.

The testing electrodes were prepared to analyze the electrochemical performance of the materials. The anode slurry consisted of 80% cathode material, 10% Carbon black SuperP, and 10% PVDF binder (Solef 5130, Syensqo, Panoli, India), while the cathode suspension comprised 92% cathode material, 5% Carbon black SuperP, and 3% PVDF binder (Solef 5130). N-Methyl pyrrolidone served as the solvent in this process. The resulting slurry was applied to copper and aluminum foils utilizing the MSK-AFA-III film coater from MTI Corp. (Richmond, CA, USA), with a clearance height of 200 µm. The electrodes were subsequently dried, rolled, and subjected to electrochemical testing in CR-2032-coin cells (Mouser Electronics India, Bengaluru, India) in a glove box filled with dry argon. Lithium foil was utilized as the anode, and a TC-E918 (Tinci, Guangzhou, China) electrolyte and two layers of Celgard 2325 separators (Celgard LLC, Charlotte, NC, USA) were employed. To determine the electrochemical characteristics of the synthesized material, the material was assembled into CR2032 layouts and evaluated using a Neware coin cell-5V 10 mA Battery Test System (Neware Technology Limited, Shenzhen, China) during charging/discharging processes. The cyclic voltammetry analysis was performed at a scan rate of 0.5 mV/s over a potential range of 0 to 2.5 V. Electrochemical impedance spectroscopy (EIS) was performed on a potentiostat Corrtest CS310 (Wuhan Corrtest Instruments Corp., Ltd., Wuhan, China) in a frequency range from 10^5 to 10^{-2} Hz. The amplitude of the voltage deviation was 5 mV. The measuring cell was a semi-element with an antielectrode in the form of lithium metal. The measurement was carried out using a two-electrode circuit at a SOC of 100%. The spectra were modeled using ZView 2 software.

3. Results

3.1. Description of the Initial Material

Figure 2 presents a diffraction pattern illustrating the preliminary cathode and anode electrodes extracted from the end-of-life lithium-ion battery. Notable peaks corresponding to lithium cobalt oxide, categorized under the space group R3-m, as well as peaks associated with graphite, classified under the space group P63/mmc, are distinctly observable.

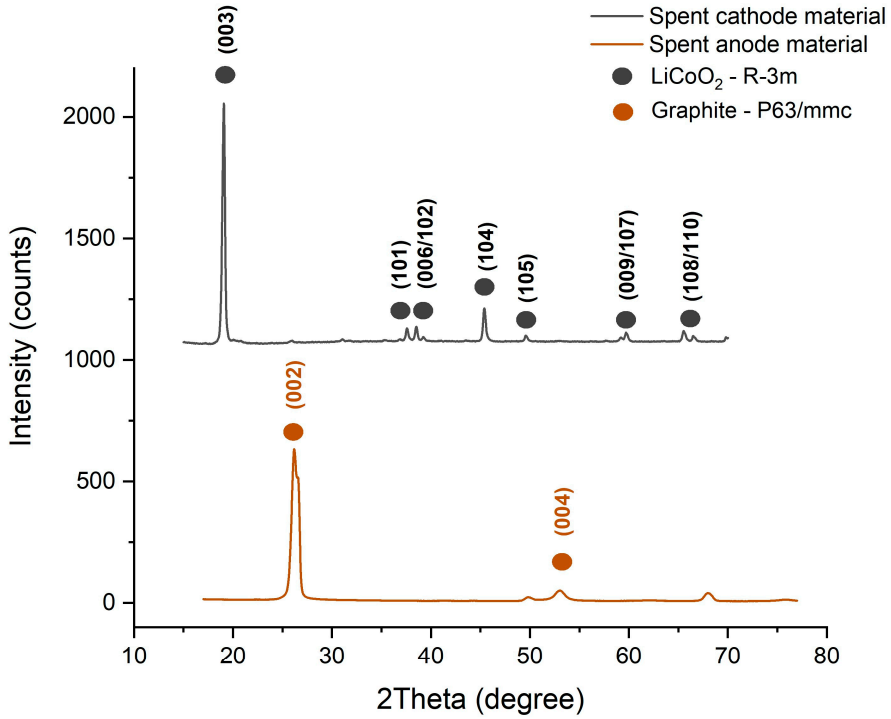


Figure 2. The diffraction pattern of the preliminary electrodes.

Table 2 presents the compositional analysis of the starting materials obtained by the EDS.

Table 2. Compositional analysis of the starting materials in atomic percent.

	C	O	F	Al	P	S	Ti	Fe	Co	Cu
Cathode	33.67	34.76	14.61	5.72	1.72	0.12	0.05	1.14	8.21	-
Anode	62.27	21.21	15.80	-	0.40	0.16	-	-	-	0.16

The EDX analysis of the cathode material revealed not only cobalt (Co), lithium (Li), and oxygen (O) from the composition of $LiCoO_2$, but also traces of aluminum (Al), carbon (C), fluorine (F), phosphorus (P), sulfur (S), titanium (Ti), and iron (Fe). These additional elements are likely associated with the presence of binder materials, electrolyte salts, and aluminum foil. Furthermore, the results of analyses indicate a significant concentration of oxygen (O), fluorine (F), phosphorus (P), and copper (Cu) on the surface of the spent graphite (SG) from the anode material. This presence is predominantly associated with the residual electrolyte, binders, organic compounds, and copper powder introduced during the liberation of active substances.

The scanning electron microscopy images of the initial materials are shown in Figure 3. Figure 3a demonstrates the spent graphite surface in secondary electron (SE) mode. Obviously, in Figure 3a, there is a presence of white substances on the graphite surface, which could be associated with metal impurities and organic residuals from PVDF or electrolyte salts. SG maintains its graphite structure despite extended charge/discharge cycles. The powder has flaky particles with an average particle size of 10–25 microns; it exhibits a uniform particle size distribution.

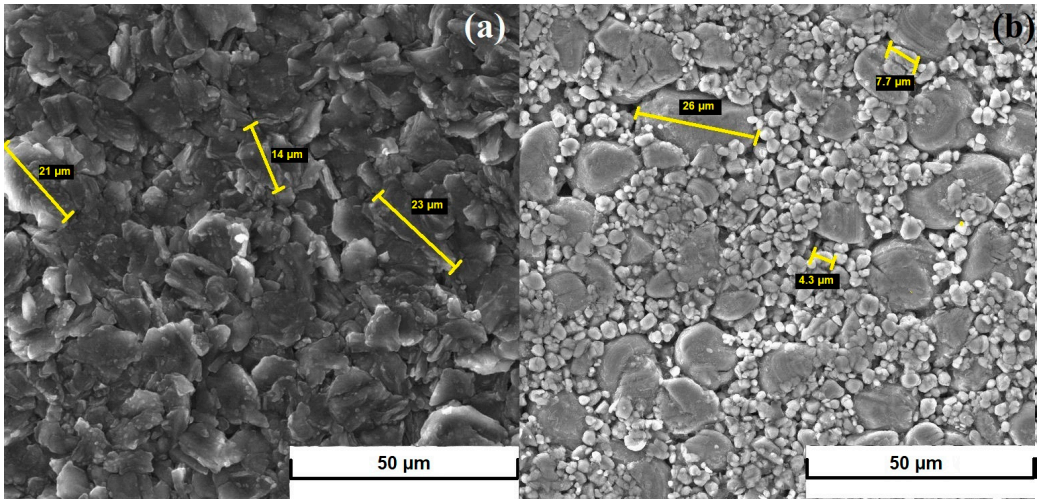


Figure 3. The SEM images of the spent materials in SE mode: (**a**)—spent anode material, (**b**)—spent cathode material.

Simultaneously in Figure 3b, the morphology of spent cathode material is illustrated. There is an obvious presence of a large number of agglomerates. The powder has rounded particles with a range of sizes from 3 mkm to 30 mkm.

3.2. Analysis of the Regenerated Graphite Material

The diffraction patterns of spent graphite (SG), leached graphite (LG), and regenerated graphite (RG) are shown in Figure 4.

Figure 4a presents the X-ray diffraction patterns of both regenerated and spent graphite within the angular range of 15–80°. The results of the magnification at the (002) plane are illustrated in Figure 4b, while the physical parameters corresponding to the detailed (002) crystal plane are provided in Table 3.

Table 3. Structural parameters of SG, LG, and RG materials at (002) peak.

	a (Å)	c (Å)	d (Å)	FWHM (°)
SG	2.460	6.713	3.356	0.571
LG	2.459	6.718	3.358	0.169
RG	2.469	6.709	3.354	0.210

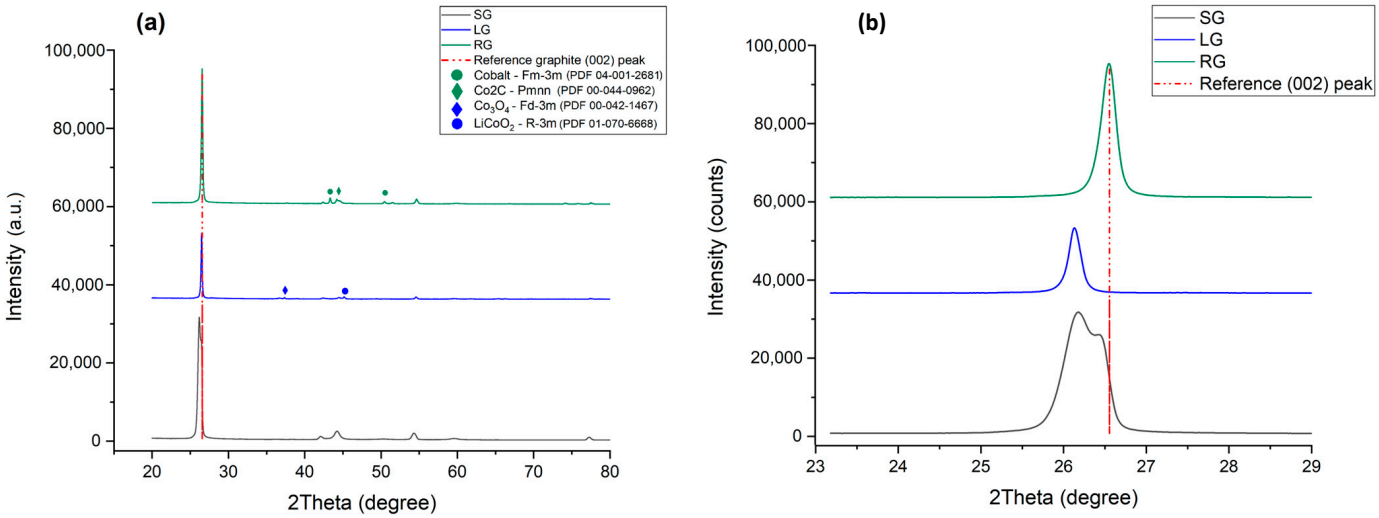


Figure 4. The diffraction patterns: (**a**) of spent graphite (SG), leached graphite (LG), and regenerated graphite (RG); (**b**) the same patterns with a large magnification in the angles 2θ.

The presence of the second peak is probably due to the presence of lithium in some parts of the anode material remaining after the intercalation of ions during the charging process. Lithium, by embedding, increases the parameter from the hexagonal structure and, thereby, shifts the peak position for a part of the material to the left. For this reason, we observe a bifurcation of peaks in the area of 26 degrees. The standard XRD patterns of LiC_x compounds and graphite, cobalt carbide, and cobalt are demonstrated in Supplementary Materials.

The characteristic interplanar spacing (d002) was approved as 3.354 Å for RG material corresponding to the complete three-dimensional ordering of the perfect graphite crystal lattice [42]. Except for these peaks, on this XRD pattern, there were additionally found peaks of cobalt and Co_2C, which are attributed to the presence of spent cathode material while joint leaching. The presence of metallic cobalt is a key factor in graphitization degree increase. The appearance of dicobalt carbide is explained by the decomposition of cobalt malate in an oxygen-free environment (Equation (1)):

$$2C_4H_6CoO_5\ (400\ ^\circ C, Ar) \rightarrow Co_2C + 3C + 4CO_2 + 6H_2O \quad (1)$$

The resulting dicobalt carbide decomposes to metallic cobalt and carbon black (Equation (2)):

$$Co_2C\ (400\ ^\circ C, CO_2) \rightarrow 2Co + C \quad (2)$$

The mixed cobalt oxide 2, 3 in the sample decomposed in an oxygen-free environment in the presence of carbon to form metallic cobalt (Equation (3)):

$$Co_3O_4 + 2C = 3Co + 2CO_2 \quad (3)$$

As illustrated in Figure 4b, the distinctive peaks corresponding to various graphite (002) surfaces exhibit notable differences. The leached graphite peak is displaced to the left in comparison to that of spent graphite, indicating that the leaching process using malic

acid results in an increase in graphite layer spacing, attributed to the intercalation of malic acid ions [43]. Following annealing, the graphite layer spacing progressively reduces due to the elimination of internal impurities and the rectification of internal defects. Consequently, the diffraction of graphite displaces to the right in the (002) plane, indicating a reduction in layer spacing as evidenced by the interplanar spacing diffraction peak.

The chemical composition of the leached and regenerated graphite is presented in the Table 4.

Table 4. Chemical composition of the leached and regenerated graphite materials in at.%.

	C	F	Al	Co	Cu	Total
LG	97.10	1.65	0.12	1.14	-	100.00
RG	99.15	-	0.27	0.37	0.21	100.00

Furthermore, it is evident that the graphite surface depicted in Figure 5a is significantly smoother than that presented in Figure 3a. The size of the graphite particles ranges from 10 to 25 µm, exhibiting a uniform size distribution, and the particles are characterized by a flaky morphology. Additionally, the presence of round particles on the surface is notable, with a size range of 300 to 1000 nanometers, which are presumably cobalt metal particles. Collectively, these scanning electron microscopy photographs indicate that high temperature annealing efficiently eliminates organic compounds, including residual binders and metal impurities, while promoting the formation of amorphous carbon and the development of new graphite microcrystals on the surface of graphite.

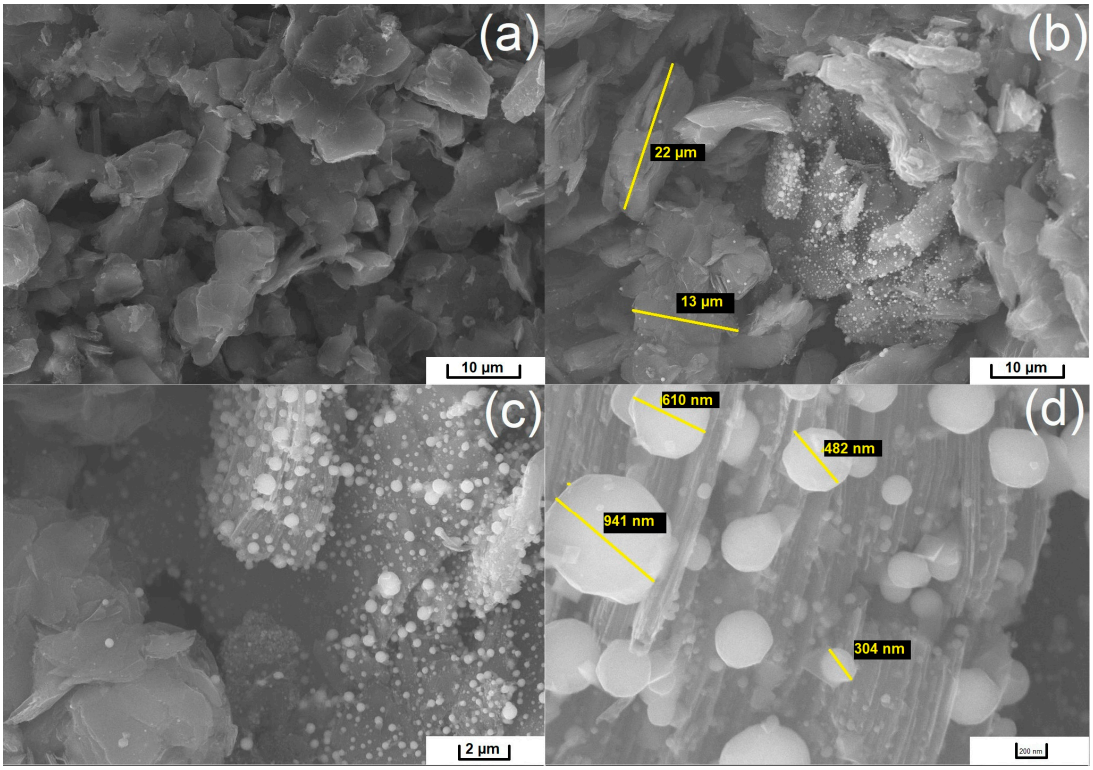


Figure 5. The SEM images of the recovered graphite material. (**a**)—LG, (**b**–**d**)—RG.

3.3. Electrochemical Performance of Graphite Material

The electrochemical features of the recovered graphite samples are presented in Figure 6. Figure 6a depicts the curve of the charge/discharge process for the first and tenth cycles at 0.1C current rate and within a voltage range of 0.01–2 V. The synthesized material exhibited a specific capacity at a charge of 447.12 mAh/g and a specific capacity

at a discharge of 364.93 mAh/g during the first cycle, resulting in a Coulombic efficiency of 81.6%. For the tenth cycle, the specific capacities were recorded at 371.9 mAh/g and 371.7 mAh/g. The Coulombic efficiency remaining close to 100% at the tenth cycle indicates the reversible intercalation/deintercalation of lithium. Additionally, a slight increase in discharge capacity during the cycling process suggests the enhancement of the active mass. The shape of the charge/discharge curves is characteristic of graphite materials.

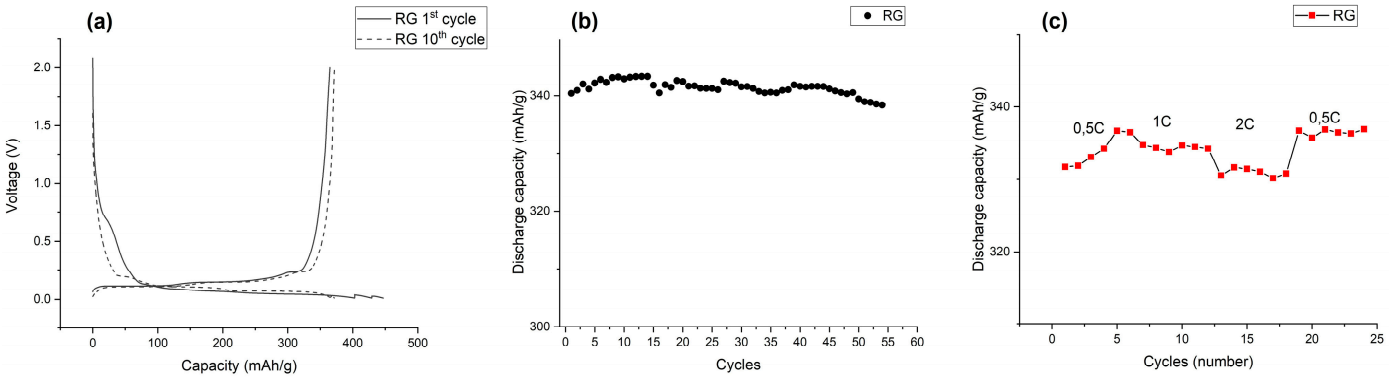


Figure 6. The analysis of the RG electrochemical performance includes (**a**) charge/discharge curves for the first and tenth cycles, (**b**) cyclic testing, and (**c**) a study on varying current loads.

The cyclic behavior of the material's resources was also examined, with results depicted in Figure 6b. In the first cycle, the discharge capacity measured 340.4 mAh/g, while in the 55th cycle, the discharge capacity was recorded at 338.4 mAh/g. The capacity loss over the course of 60 cycles amounted to 0.59%. These findings indicate the stability of the regenerated graphite structure.

Furthermore, for the regenerated materials, a current load study was conducted followed by a relaxation phase to evaluate the structural stability of the material. Results from this investigation are shown in Figure 6c. The material was tested with discharge currents corresponding to two-hour, one-hour, and thirty-minute cycles. The initial discharge was performed at a current of 0.5C for the first five cycles. Compared to the two-hour discharge cycle, capacity decreased by 0.7% at 1C and by 1.8% at 2C. Following 24 cycles of current load, when discharged at a current of 0.5C, the material exhibited capacity values approaching the initial levels, indicating that the material demonstrates considerable stability.

Figure 7 demonstrates the polarization curves of the regenerated graphite and commercial graphite (CG) obtained by cyclic voltammogram. In the cyclic voltammetry (CV) curve of the initial cycle, the reduction peak observed in Figure 7b at 0.5 V indicates the irreversible process of solid electrolyte interphase (SEI) film formation [44]. In the detailed cycle CV curve, the reduction peak near 0.2 V indicates the intercalation of lithium ions, while the oxidation peak around 0.4 V signifies the extraction of lithium ions [45,46]. In turn, RG polarization curves in Figure 7a demonstrate only the reduction peak around 0.1 V, which is the sign of lithium intercalation, and an oxidation peak in the region of 0.4 V, signifying the process of lithium deintercalation. Moreover, the reduction peak of RG closely matches that of CG, suggesting that the graphite defects were effectively restored after purification and regeneration.

The impedance spectrum of the graphite layout, as well as its equivalent circuit, is presented in Figure 8.

In the presented spectrum, two semicircles are obvious, which are modeled by elements R2/C1 and R3/CPU 2, corresponding to the SEI characteristic responses and charge transfer, as well as a straight section associated with diffusion processes. The resistance R1 simulates the internal resistance of the cell. The parameters of the equivalent scheme are shown in Table 5.

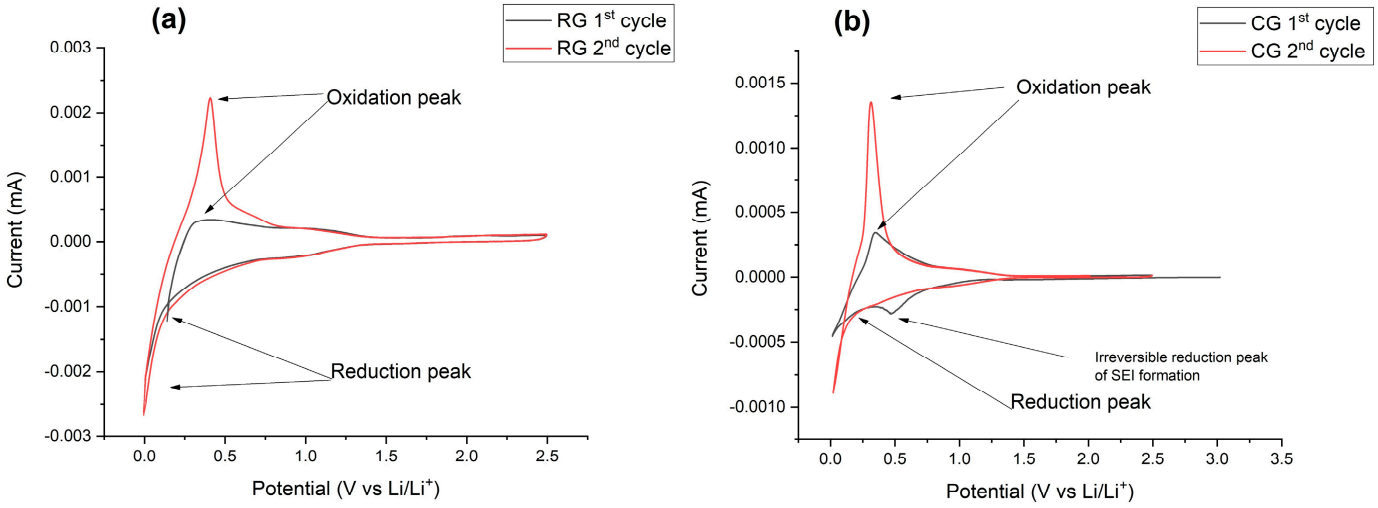


Figure 7. CVA curves of RG (**a**) and CG (**b**).

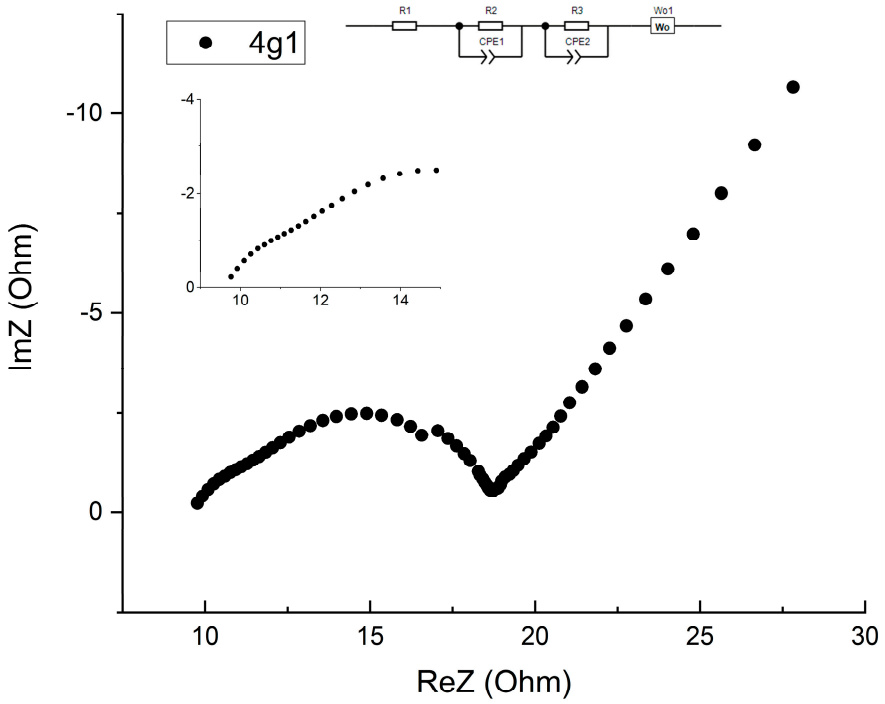


Figure 8. The impedance spectrum of the graphite layout and its equivalent circuit.

Table 5. The parameters of equivalent scheme.

R1, Ω	R2, Ω	C1, F	R3, Ω	C2, F
9.05	4.04	1.40×10^{-3}	5.31	4.00×10^{-4}

3.4. Analysis of Synthesized NCM Material

The elemental composition of the synthesized triple-lithiated cathode material was analyzed utilizing energy-dispersive X-ray spectroscopy. The results are shown in Table 6.

Table 6. The elemental composition of synthesized NCM material in at. %.

Element	Ni	Co	Mn	O	P	Al	Total
at. %	19.25	18.16	21.87	35.36	0.23	5.11	100

The atomic ratio of transition metals in the synthesized material, $Li(Ni_{0.32}\ Co_{0.31}\ Mn_{0.37})O_2$, is closely aligned with the theoretically calculated composition of NCM111. However, the concentrations of cobalt and nickel in the synthesized material are slightly lower than those predicted theoretically, resulting in an altered atomic ratio that favors the addition of manganese. In NCM-type materials, manganese contributes to stability by promoting the formation of a spinel structure, which facilitates low internal resistance but is associated with reduced specific energy; this characteristic is beneficial when combined with nickel, which is characterized by high specific energy but relatively poor stability. Conversely, a lower content of nickel and cobalt may compromise these desirable characteristics.

Figure 9 presents the findings of the morphological analysis of the synthesized NCM sample, which was conducted using SEM in SE mode. It is evident that the agglomeration of particles within the sample is significant, with the agglomerates exhibiting an average size ranging from 20 to 50 microns and demonstrating a uniform particle size distribution. At an increased magnification, it is evident that the agglomerates are made up of rounded particles averaging between 0.25 and 0.45 microns in size. This small particle size and uniform distribution promote the rapid migration of Li^+ ions, which may enhance the electrochemical properties [47].

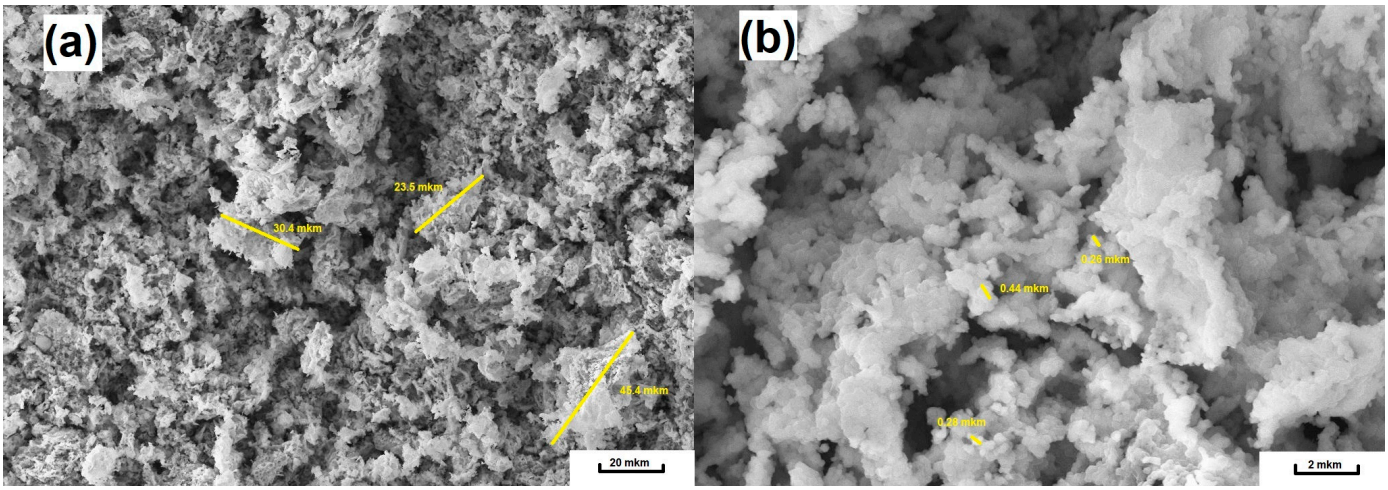


Figure 9. SEM photographs of SNCM. (**a**) at magnification ×1.5 K; (**b**) at magnification ×5 K.

Figure 10 presents the diffraction pattern of an obtained cathode material designated as NCM111, which is indexed to a layered oxide exhibiting an R-3m space group, with no observable peaks associated with impurity phases. The peaks align with the standard card for $Li(Ni_1/3Co_{1/3}Mn_{1/3})O_2$ (PDF#01-075-9200). The pronounced peak splitting corresponding to the (006)/(102) planes indicates the presence of a well-ordered layered structure.

Also, it is extremely recommended for such type of materials to analyze the following parameters [48–50]:

1. The separation of the peaks I006/I102 (around 2θ~36°) indicates a favorable ordering of the hexagonal lattice, with peak separation evident in the synthesized NCM.
2. The R-factor, defined as R = (I006 + I102)/I101, reflects structural ordering; a lower value indicates better ordering, with values below 0.5 suggesting high-quality materials. For the synthesized sample, this value is 0.929, exceeding the desirable threshold. The R-factor is notably high for this type of material, likely due to the influence of sol–gel synthesis on powder morphology. The ratio of the 003 and 104 peaks indicates that the crystal lattice of the SNCM is hexagonal.
3. The ratio I003/I104 (with 2θ 003~20° and 2θ 104~45°) assesses the cubic nature of the lattice, where a smaller ratio implies a closer alignment with a cubic structure. In

this case, the parameter reflects cationic mixing, with values over 1.2 indicative of high-quality materials. The SNCM shows a ratio of 1.565.

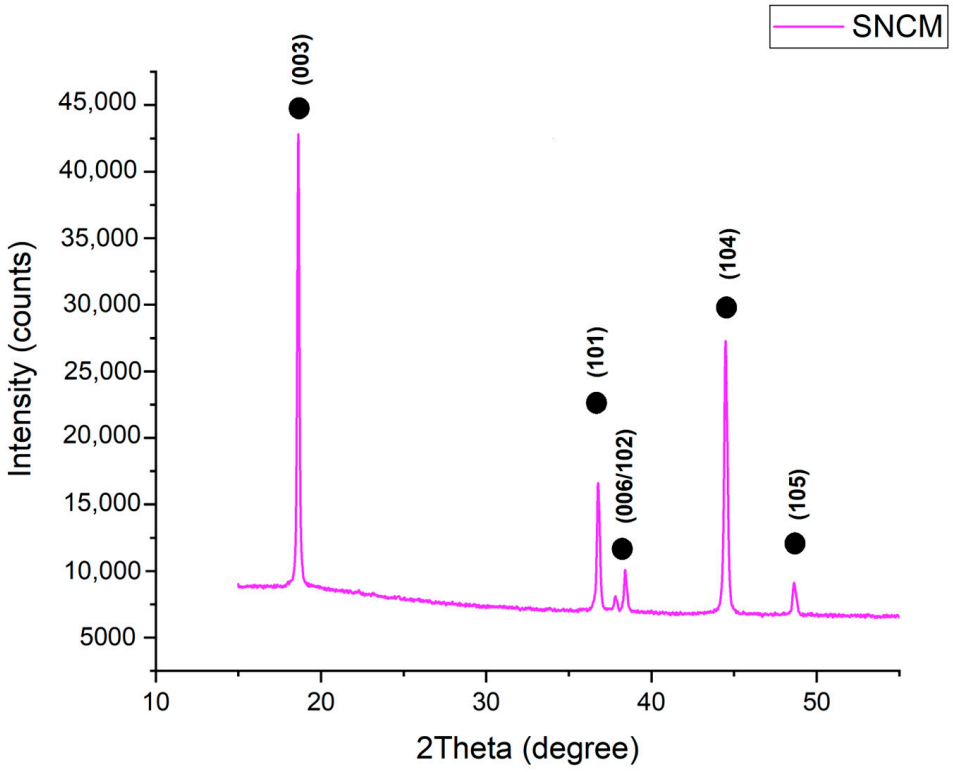


Figure 10. XRD pattern of SNCM material.

3.5. Electrochemical Performance of SNCM

The electrochemical behavior of SNCM material is demonstrated in Figure 11. Figure 11a shows the curve of the charge/discharge process on the 1st and 10th cycles at 0.1C and in the voltage range 2.8–4.3 V. The obtained material demonstrated a specific charge capacity of 155.71 mAh/g, and a capacity at discharge of 131.69 mAh/g, for the 10th cycle—124.13 and 121.61, respectively. The Coulomb efficiency on the first cycle of the material was 84.5%, and on the 10th cycle—98.0%. The low value on the 1st cycle is explained by the CEI formation, as there is probably a large specific surface area and a lot of carbon black; these factors perhaps may be an explanation for low material efficiency—a large surface for the formation of the CEI layer. The rise in the value to nearly 100% during the next charge/discharge cycles indicates reversible intercalation/deintercalation of lithium.

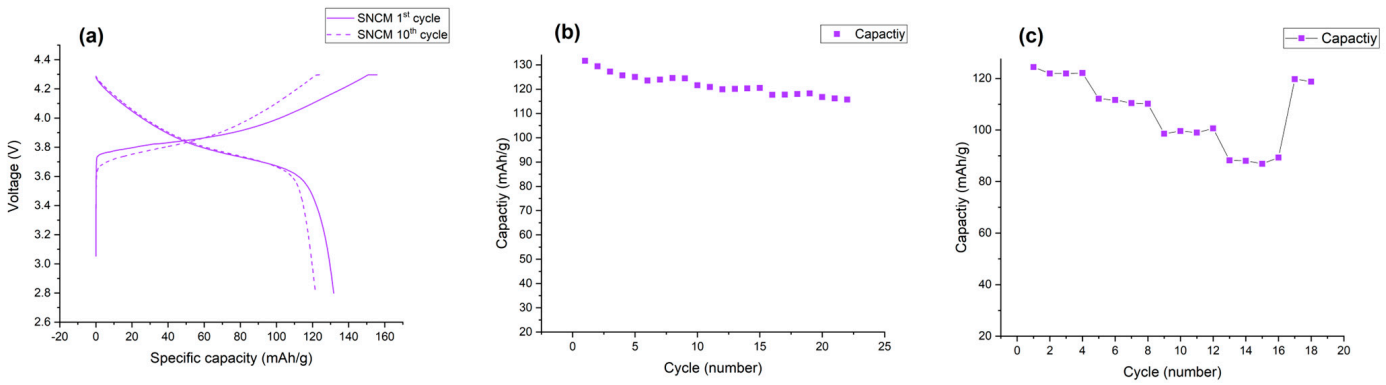


Figure 11. The electrochemical behavior of the SNCM. (**a**)—charge/discharge curves on 1st and 10th cycles, (**b**)—cyclic test, (**c**)—t current load study.

The cyclic behavior of the material was also examined, as illustrated in Figure 11b. In the first cycle, the discharge capacities were recorded at 130.73 mAh/g and 115.74 mAh/g on the twenty-second cycle. The capacity degradation observed over the course of 60 cycles amounted to 11.5%. This decline in capacity during cycling can be attributed to a relatively high R-factor value of 0.929, indicating that the structure of the sample is not well-ordered.

Additionally, a study on current loading was performed on the synthesized material, followed by a relaxation phase to evaluate its structural stability; the findings are shown in Figure 11c. The material was evaluated with discharge currents corresponding to durations of twenty hours, three hours, one hour, and thirty minutes. The first four cycles were conducted at a current of 0.05C. Capacity reductions compared to the twenty-hour discharge cycle were observed as 11.2% at 0.3C, 19.9% at 1C, and 29.6% at 1.5C. After 18 cycles of current loading, discharging at 0.05C resulted in capacity values similar to the initial measurements, indicating a strong level of stability.

4. Conclusions

This paper outlines the process of graphite regeneration from spent anodes and the simultaneous synthesis of triple-lithiated transition metal oxide NCM111 from spent $LiCoO_2$, utilizing previously developed methodologies for the extraction of valuable metals from spent anodes and cathodes derived from end-of-life lithium-ion batteries, followed by heat treatment processes for graphite in an argon atmosphere and for NCM in an air atmosphere. The resulting graphite material was examined using various methods, including X-ray diffraction (XRD), scanning electron microscopy (SEM), energy-dispersive X-ray spectroscopy (EDS), charge/discharge tests, cyclic voltammetry (CVA), and electrochemical impedance spectroscopy (EIS). The initial capacity of the regenerated graphite (RG) was measured at 340.4 mAh/g, maintaining a capacity of 338.4 mAh/g after 55 cycles at a current rate of 0.1C. These results align with the specifications for commercial materials of the same type. The cycle life assessment of the material indicates a reduction of only 0.6% after 55 cycles, demonstrating the stability of the graphite structure, as corroborated by the current load study. The polarization curves of RG exhibited symmetric peaks indicative of reversible redox reactions within the voltage range of 0 to 2.5 V. Moreover, no evidence of an irreversible reduction peak associated with the formation of the solid electrolyte interface (SEI) was observed in comparison to commercial graphite (CG), which facilitated the achievement of high Coulomb efficiency values during the first cycle.

Additionally, the NCM111 was synthesized based on the solution from the extraction process. This material was also analyzed by SEM, EDS, XRD, and electrochemical tests. The obtained results of capacity and cycle resource were unsatisfactory because of the unordered structure of SNCM. In further research, it is planned to change the type of synthesis from sol–gel to co-precipitation in order to achieve the perfect electrochemical characteristics of the material.

Nevertheless, the developed strategy allows for the shortening of the regeneration process of spent cathode and anode materials and solving of the essential problem of production scale recycling processes—how to divide cathode and anode materials from the "black mass".

Supplementary Materials: The following supporting information can be downloaded at: https://www.mdpi.com/article/10.3390/en17225570/s1, Figure S1: The diagram of the heat treatment stages; Figure S2: The standard XRD patterns of LiC_x and graphite; Figure S3: The standard XRD pattern of the cobalt carbide; Figure S4: The standard XRD pattern of the cobalt.

Author Contributions: Conceptualization, A.K. and K.P.; methodology, A.K. and K.P.; formal analysis, A.K.; investigation, A.K., K.P. and V.C.; resources, A.A.P.; data curation, A.K. and K.P.; writing—original draft preparation, A.K.; writing—review and editing, V.C.; visualization, A.K.; supervision, P.N.; project administration, P.N. and A.A.P.; funding acquisition, A.A.P. All authors have read and agreed to the published version of the manuscript.

Funding: The research was funded by the Ministry of Science and Higher Education of the Russian Federation by «Agreement on the grant in the form of subsidies from the federal budget for the implementation of state support for the creation and development of world-class scientific centers, those are performing research and development on the priorities of scientific and technological development» dated 20 April 2022 No. 075-15-2022-311.

Data Availability Statement: The original contributions presented in the study are included in the article/Supplementary Materials, further inquiries can be directed to the corresponding author.

Conflicts of Interest: The authors declare no conflicts of interest.

References

1. Han, X.; Lu, L.; Zheng, Y.; Feng, X.; Li, Z.; Li, J.; Ouyang, M. A Review on the Key Issues of the Lithium Ion Battery Degradation among the Whole Life Cycle. *eTransportation* **2019**, *1*, 100005. [CrossRef]
2. Zhang, X.; Shi, H.; Tan, N.; Zhu, M.; Tan, W.; Daramola, D.; Gu, T. Advances in Bioleaching of Waste Lithium Batteries under Metal Ion Stress. *Bioresour. Bioprocess.* **2023**, *10*, 19. [CrossRef] [PubMed]
3. Qu, X.; Cai, M.; Zhang, B.; Xie, H.; Guo, L.; Wang, D.; Yin, H. A Vapor Thermal Approach to Selective Recycling of Spent Lithium-Ion Batteries. *Green Chem.* **2021**, *23*, 8673–8684. [CrossRef]
4. Assefi, M.; Maroufi, S.; Yamauchi, Y.; Sahajwalla, V. Pyrometallurgical Recycling of Li-Ion, Ni–Cd and Ni–MH Batteries: A Minireview. *Curr. Opin. Green Sustain. Chem.* **2020**, *24*, 26–31. [CrossRef]
5. Cao, Z.; Zheng, X.; Cao, H.; Zhao, H.; Sun, Z.; Guo, Z.; Wang, K.; Zhou, B. Efficient Reuse of Anode Scrap from Lithium-Ion Batteries as Cathode for Pollutant Degradation in Electro-Fenton Process: Role of Different Recovery Processes. *Chem. Eng. J.* **2018**, *337*, 256–264. [CrossRef]
6. Cheng, H.; Shapter, J.G.; Li, Y.; Gao, G. Recent Progress of Advanced Anode Materials of Lithium-Ion Batteries. *J. Energy Chem.* **2021**, *57*, 451–468. [CrossRef]
7. Zhang, H.; Yang, Y.; Ren, D.; Wang, L.; He, X. Graphite as Anode Materials: Fundamental Mechanism, Recent Progress and Advances. *Energy Storage Mater.* **2021**, *36*, 147–170. [CrossRef]
8. Gao, Y.; Wang, C.; Zhang, J.; Jing, Q.; Ma, B.; Chen, Y.; Zhang, W. Graphite Recycling from the Spent Lithium-Ion Batteries by Sulfuric Acid Curing–Leaching Combined with High-Temperature Calcination. *ACS Sustain. Chem. Eng.* **2020**, *8*, 9447–9455. [CrossRef]
9. Yi, C.; Yang, Y.; Zhang, T.; Wu, X.; Sun, W.; Yi, L. A Green and Facile Approach for Regeneration of Graphite from Spent Lithium Ion Battery. *J. Clean. Prod.* **2020**, *277*, 123585. [CrossRef]
10. Yi, C.; Zhou, L.; Wu, X.; Sun, W.; Yi, L.; Yang, Y. Technology for Recycling and Regenerating Graphite from Spent Lithium-Ion Batteries. *Chin. J. Chem. Eng.* **2021**, *39*, 37–50. [CrossRef]
11. Qiao, Y.; Zhao, H.; Shen, Y.; Li, L.; Rao, Z.; Shao, G.; Lei, Y. Recycling of Graphite Anode from Spent Lithium-ion Batteries: Advances and Perspectives. *EcoMat* **2023**, *5*, e12321. [CrossRef]
12. Larcher, D.; Tarascon, J.-M. Towards Greener and More Sustainable Batteries for Electrical Energy Storage. *Nat. Chem.* **2015**, *7*, 19–29. [CrossRef] [PubMed]
13. Abdollahifar, M.; Doose, S.; Cavers, H.; Kwade, A. Graphite Recycling from End-of-Life Lithium-Ion Batteries: Processes and Applications. *Adv. Mater. Technol.* **2023**, *8*, 2200368. [CrossRef]
14. Kosenko, A.; Pushnitsa, K.; Pavlovskii, A.A.; Novikov, P.; Popovich, A.A. The Review of Existing Strategies of End-of-Life Graphite Anode Processing Using 3Rs Approach: Recovery, Recycle, Reuse. *Batteries* **2023**, *9*, 579. [CrossRef]
15. Yu, H.; Dai, H.; Zhu, Y.; Hu, H.; Zhao, R.; Wu, B.; Chen, D. Mechanistic Insights into the Lattice Reconfiguration of the Anode Graphite Recycled from Spent High-Power Lithium-Ion Batteries. *J. Power Sources* **2021**, *481*, 229159. [CrossRef]
16. Rothermel, S.; Evertz, M.; Kasnatscheew, J.; Qi, X.; Grützke, M.; Winter, M.; Nowak, S. Graphite Recycling from Spent Lithium-Ion Batteries. *ChemSusChem* **2016**, *9*, 3473–3484. [CrossRef]
17. Yuwen, C.; Liu, B.; Zhang, H.; Tian, S.; Zhang, L.; Guo, S.; Zhou, B. Efficient Recovery and Regeneration of Waste Graphite through Microwave Stripping from Spent Batteries Anode for High-Performance Lithium-Ion Batteries. *J. Clean. Prod.* **2022**, *333*, 130197. [CrossRef]
18. Li, Z.; Li, S.; Wang, T.; Yang, K.; Zhou, Y.; Tian, Z. Facile Fabrication of High-Performance Li-Ion Battery Carbonaceous Anode from Li-Ion Battery Waste. *J. Electrochem. Soc.* **2021**, *168*, 090513. [CrossRef]
19. Da, H.; Gan, M.; Jiang, D.; Xing, C.; Zhang, Z.; Fei, L.; Cai, Y.; Zhang, H.; Zhang, S. Epitaxial Regeneration of Spent Graphite Anode Material by an Eco-Friendly In-Depth Purification Route. *ACS Sustain. Chem. Eng.* **2021**, *9*, 16192–16202. [CrossRef]
20. Ma, Z.; Zhuang, Y.; Deng, Y.; Song, X.; Zuo, X.; Xiao, X.; Nan, J. From Spent Graphite to Amorphous Sp^2 + sp^3 Carbon-Coated Sp 2 Graphite for High-Performance Lithium Ion Batteries. *J. Power Sources* **2018**, *376*, 91–99. [CrossRef]
21. Zhang, J.; Li, X.; Song, D.; Miao, Y.; Song, J.; Zhang, L. Effective Regeneration of Anode Material Recycled from Scrapped Li-Ion Batteries. *J. Power Sources* **2018**, *390*, 38–44. [CrossRef]
22. Ye, L.; Wang, C.; Cao, L.; Xiao, H.; Zhang, J.; Zhang, B.; Ou, X. Effective Regeneration of High-Performance Anode Material Recycled from the Whole Electrodes in Spent Lithium-Ion Batteries via a Simplified Approach. *Green Energy Environ.* **2021**, *6*, 725–733. [CrossRef]

23. Zhao, T.; Yao, Y.; Wang, M.; Chen, R.; Yu, Y.; Wu, F.; Zhang, C. Preparation of MnO_2-Modified Graphite Sorbents from Spent Li-Ion Batteries for the Treatment of Water Contaminated by Lead, Cadmium, and Silver. *ACS Appl. Mater. Interfaces* **2017**, *9*, 25369–25376. [CrossRef] [PubMed]
24. Hao, J.; Meng, X.; Fang, S.; Cao, H.; Lv, W.; Zheng, X.; Liu, C.; Chen, M.; Sun, Z. MnO_2-Functionalized Amorphous Carbon Sorbents from Spent Lithium-Ion Batteries for Highly Efficient Removal of Cadmium from Aqueous Solutions. *Ind. Eng. Chem. Res.* **2020**, *59*, 10210–10220. [CrossRef]
25. Divya, M.L.; Natarajan, S.; Lee, Y.-S.; Aravindan, V. Achieving High-Energy Dual Carbon Li-Ion Capacitors with Unique Low- and High-Temperature Performance from Spent Li-Ion Batteries. *J. Mater. Chem. A* **2020**, *8*, 4950–4959. [CrossRef]
26. Liang, H.-J.; Hou, B.-H.; Li, W.-H.; Ning, Q.-L.; Yang, X.; Gu, Z.-Y.; Nie, X.-J.; Wang, G.; Wu, X.-L. Staging Na/K-Ion de-/Intercalation of Graphite Retrieved from Spent Li-Ion Batteries: In Operando X-Ray Diffraction Studies and an Advanced Anode Material for Na/K-Ion Batteries. *Energy Environ. Sci.* **2019**, *12*, 3575–3584. [CrossRef]
27. Yang, J.-L.; Zhao, X.-X.; Li, W.-H.; Liang, H.-J.; Gu, Z.-Y.; Liu, Y.; Du, M.; Wu, X.-L. Advanced Cathode for Dual-Ion Batteries: Waste-to-Wealth Reuse of Spent Graphite from Lithium-Ion Batteries. *eScience* **2022**, *2*, 95–101. [CrossRef]
28. Meng, Y.-F.; Liang, H.-J.; Zhao, C.-D.; Li, W.-H.; Gu, Z.-Y.; Yu, M.-X.; Zhao, B.; Hou, X.-K.; Wu, X.-L. Concurrent Recycling Chemistry for Cathode/Anode in Spent Graphite/$LiFePO_4$ Batteries: Designing a Unique Cation/Anion-Co-Workable Dual-Ion Battery. *J. Energy Chem.* **2022**, *64*, 166–171. [CrossRef]
29. Divya, M.L.; Lee, Y.; Aravindan, V. Li-ion Capacitor via Solvent-Co-Intercalation Process from Spent Li-ion Batteries. *Batter. Supercaps* **2021**, *4*, 671–679. [CrossRef]
30. Kurian, M. Recent Progress in the Chemical Reduction of Graphene Oxide by Green Reductants—A Mini Review. *Carbon Trends* **2021**, *5*, 100120. [CrossRef]
31. Sun, X.; Huang, C.; Wang, L.; Liang, L.; Cheng, Y.; Fei, W.; Li, Y. Recent Progress in Graphene/Polymer Nanocomposites. *Adv. Mater.* **2021**, *33*, 2001105. [CrossRef] [PubMed]
32. Guan, J.; Li, Z.; Chen, S.; Gu, W. Zero-Valent Iron Supported on Expanded Graphite from Spent Lithium-Ion Battery Anodes and Ferric Chloride for the Degradation of 4-Chlorophenol in Water. *Chemosphere* **2022**, *290*, 133381. [CrossRef] [PubMed]
33. Badawy, S.M. Synthesis of High-quality Graphene Oxide from Spent Mobile Phone Batteries. *Environ. Prog. Sustain. Energy* **2016**, *35*, 1485–1491. [CrossRef]
34. Wang, Y.; Cao, H.; Chen, L.; Chen, C.; Duan, X.; Xie, Y.; Song, W.; Sun, H.; Wang, S. Tailored Synthesis of Active Reduced Graphene Oxides from Waste Graphite: Structural Defects and Pollutant-Dependent Reactive Radicals in Aqueous Organics Decontamination. *Appl. Catal. B Environ.* **2018**, *229*, 71–80. [CrossRef]
35. Xu, Q.; Wang, Y.; Shi, X.; Zhong, Y.; Wu, Z.; Song, Y.; Wang, G.; Liu, Y.; Zhong, B.; Guo, X. The Direct Application of Spent Graphite as a Functional Interlayer with Enhanced Polysulfide Trapping and Catalytic Performance for Li–S Batteries. *Green Chem.* **2021**, *23*, 942–950. [CrossRef]
36. Zhao, L.; Liu, X.; Wan, C.; Ye, X.; Wu, F. Soluble Graphene Nanosheets from Recycled Graphite of Spent Lithium Ion Batteries. *J. Mater. Eng. Perform.* **2018**, *27*, 875–880. [CrossRef]
37. Natarajan, S.; Bhattarai, R.M.; Sudhakaran, M.S.P.; Mok, Y.S.; Kim, S.J. Recycling of Spent Graphite and Copper Current Collector for Lithium-Ion and Sodium-Ion Batteries. *J. Power Sources* **2023**, *577*, 233170. [CrossRef]
38. Li, Y.; Lv, W.; Zhao, H.; Xie, Y.; Ruan, D.; Sun, Z. Regeneration of Anode Materials from Complex Graphite Residue in Spent Lithium-Ion Battery Recycling Process. *Green Chem.* **2022**, *24*, 9315–9328. [CrossRef]
39. Yu, G.-Q.; Xie, M.-Z.; Zheng, Z.-H.; Wu, Z.-G.; Zhao, H.-L.; Liu, F.-Q. Efficiently Regenerating Spent Lithium Battery Graphite Anode Materials through Heat Treatment Processes for Impurity Dissipation and Crystal Structure Repair. *Resour. Conserv. Recycl.* **2023**, *199*, 107267. [CrossRef]
40. Chen, Q.; Huang, L.; Liu, J.; Luo, Y.; Chen, Y. A New Approach to Regenerate High-Performance Graphite from Spent Lithium-Ion Batteries. *Carbon* **2022**, *189*, 293–304. [CrossRef]
41. Xie, X.; Fan, W.; Zhang, J.; Ma, R.; Chen, Y.; Wang, C. Regeneration of Graphite Anode from Spent Lithium Iron Phosphate Batteries: Microstructure and Morphology Evolution at Different Thermal-Repair Temperature. *Powder Technol.* **2023**, *430*, 118998. [CrossRef]
42. Franklin, R.E. The Structure of Graphitic Carbons. *Acta Crystallogr.* **1951**, *4*, 253–261. [CrossRef]
43. Pei, S.; Wei, Q.; Huang, K.; Cheng, H.-M.; Ren, W. Green Synthesis of Graphene Oxide by Seconds Timescale Water Electrolytic Oxidation. *Nat. Commun.* **2018**, *9*, 145. [CrossRef] [PubMed]
44. Leroy, S.; Blanchard, F.; Dedryvère, R.; Martinez, H.; Carré, B.; Lemordant, D.; Gonbeau, D. Surface Film Formation on a Graphite Electrode in Li-ion Batteries: AFM and XPS Study. *Surf. Interface Anal.* **2005**, *37*, 773–781. [CrossRef]
45. Heiskanen, S.K.; Kim, J.; Lucht, B.L. Generation and Evolution of the Solid Electrolyte Interphase of Lithium-Ion Batteries. *Joule* **2019**, *3*, 2322–2333. [CrossRef]
46. Liu, D.; Qu, X.; Zhang, B.; Zhao, J.; Xie, H.; Yin, H. Alkaline Roasting Approach to Reclaiming Lithium and Graphite from Spent Lithium-Ion Batteries. *ACS Sustain. Chem. Eng.* **2022**, *10*, 5739–5747. [CrossRef]
47. Zhang, J.; Qiao, J.; Sun, K.; Wang, Z. Balancing Particle Properties for Practical Lithium-Ion Batteries. *Particuology* **2022**, *61*, 18–29. [CrossRef]
48. Reimers, J.N.; Li, W.; Dahn, J.R. Short-Range Cation Ordering in $Li_xNi_{2-x}O_2$. *Phys. Rev. B* **1993**, *47*, 8486–8493. [CrossRef]

49. Skvortsova, I.; Savina, A.A.; Orlova, E.D.; Gorshkov, V.S.; Abakumov, A.M. Microwave-Assisted Hydrothermal Synthesis of Space Fillers to Enhance Volumetric Energy Density of NMC811 Cathode Material for Li-Ion Batteries. *Batteries* **2022**, *8*, 67. [CrossRef]
50. Zybert, M.; Ronduda, H.; Dąbrowska, K.; Ostrowski, A.; Sobczak, K.; Moszyński, D.; Hamankiewicz, B.; Rogulski, Z.; Raróg-Pilecka, W.; Wieczorek, W. Suppressing Ni/Li Disordering in $LiNi_{0.6}Mn_{0.2}Co_{0.2}O_2$ Cathode Material for Li-Ion Batteries by Rare Earth Element Doping. *Energy Rep.* **2022**, *8*, 3995–4005. [CrossRef]

Disclaimer/Publisher's Note: The statements, opinions and data contained in all publications are solely those of the individual author(s) and contributor(s) and not of MDPI and/or the editor(s). MDPI and/or the editor(s) disclaim responsibility for any injury to people or property resulting from any ideas, methods, instructions or products referred to in the content.